



# Surrogate modeling of articular cartilage degradation to understand the synergistic role of MMP-1 and MMP-9: a case study

Tanvir R. Faisal<sup>1</sup> · Malek Adouni<sup>2</sup> · Yasin Y. Dhaher<sup>3,4,5</sup>

Received: 14 November 2021 / Accepted: 22 August 2022  
© The Author(s), under exclusive licence to Springer-Verlag GmbH Germany, part of Springer Nature 2022

## Abstract

A characteristic feature of arthritic diseases is cartilage extracellular matrix (ECM) degradation, often orchestrated by the overexpression of matrix metalloproteinases (MMPs) and other proteases. The interplay between fibril level degradation and the tissue-level aggregate response to biomechanical loading was explored in this work by a computational multiscale cartilaginous model. We considered the relative abundance of collagenases (MMP-1) and gelatinases (MMP-9) in surrogate models, where the diffusion (spatial distribution) of these enzymes and the subsequent, co-localized fibrillar damage were spatially randomized with Latin Hypercube Sampling. The computational model was constructed by incorporating the results from prior molecular dynamics simulations (tensile test) of microfibril degradation into a hyper-elastoplastic fibril-reinforced cartilage model. Including MMPs-mediated collagen fibril-level degradation in computational models may help understand the ECM pathomechanics at the tissue level. The mechanics of cartilage tissue and fibril show variations in mechanical integrity depending on the different combinations of MMPs-1 and 9 with a concentration ratio of 1:1, 3:1, and 1:3 in simulated indentation tests. The fibril yield (local failure) was initiated at  $20.2 \pm 3.0$  (%) and at  $23.0 \pm 2.8$  (%) of bulk strain for col 1:gel 3 and col 3: gel 1, respectively. The reduction in failure stress (global response) was 39.8% for col 1:gel 3, 37.5% for col 1:gel 1, and 36.7% for col 3:gel 1 compared with the failure stress of the degradation free tissue. These findings indicate that cartilage's global and local mechanisms of failure largely depend on the relative abundance of the two key enzymes—collagenase (MMP-1) and gelatinase (MMP-9) and the spatial characteristics of diffusion across the layers of the cartilage ECM.

**Keywords** Cartilage degradation · Matrix metalloproteinases · MMP-1 · MMP-9 · Multiscale modeling

## 1 Introduction

Epidemiological studies indicate that either disease (Barbour et al. 2013) or trauma (Punzi et al. 2016) to the articular cartilage stimulates the production of matrix metalloproteinases

(MMPs). While MMPs are important regulators for tissue homeostasis, uncontrolled MMPs activity becomes destructive and leads to homeostasis breakdown. It has been proposed that the damage inflicted by these enzymes, initiated at the surface layer of the cartilage, is expressed during the early stages of osteoarthritis (OA) (Buckwalter and Mankin 1998; Panula et al. 1998; Weiss and Mirow 1972) and is believed to be the point of no return for disease progression (Buckwalter and Mankin 1998).

Two classes of enzymes, collagenases and gelatinases, take part in collagen degradation. It has been reported that MMP-1 (a collagenase) cleaves and binds to the triple-helical collagen molecule and denatures the collagen fibrils (Malaspina et al. 2017; Powell et al. 2019; Rosenblum et al. 2010; Sarkar et al. 2012). The initial cleavage unwinds the triple helix, which is subsequently exposed to MMP-9 (gelatinase) that plays a crucial role in the digestion of the triple helix fragments. Our prior simulation results indicate

✉ Tanvir R. Faisal  
tanvir.faisal@louisiana.edu

<sup>1</sup> Department of Mechanical Engineering, University of Louisiana at Lafayette, Lafayette, LA 70508, USA

<sup>2</sup> Department of Mechanical Engineering, Australian College of Kuwait, East Mishref, Kuwait City, P.O. Box 1411, Kuwait

<sup>3</sup> Department of Physical Medicine and Rehabilitation, University of Texas Southwest, Dallas, TX, USA

<sup>4</sup> Department of Orthopedic Surgery, University of Texas Southwest, Dallas, TX, USA

<sup>5</sup> Department of Biomedical Engineering, University of Texas Southwest, Dallas, TX, USA

that the synergistic action of these two enzymes is complex and varies with the relative abundance of the enzymes in and around the collagen fibrils (Powell et al. 2019). Therefore, the current study aims to understand the impact of this synergistic action on the aggregate biomechanical properties of articular cartilage at the tissue level.

The relationship between degraded matrix constituents and the mechanical integrity of cartilage was discreetly investigated *in vitro* through enzymatic exposure paradigms, one enzyme at a time (Grenier et al. 2014; Mixon et al. 2021; Saarakkala et al. 2004; Schmidt et al. 1990; Töyräs et al. 1999; Wang et al. 2008). However, *in vitro* degradation models to assess the mixed effect of multiple enzymes are experimentally challenging. In this context, computational models can provide unique insights into the degradation mechanisms and their effects on fibril integrity. Recently, we developed a Molecular Dynamics (MD)-based mechanistic computational framework on exploring the synergistic action of two key enzymes in the degradation of the microfibril (Powell et al. 2019). It is not clear, how the enzyme-mediated changes at the fibril level are manifested in the tissue level mechanics.

Thus, in this study, the interplay between fibril level degradation and aggregate mechanics will be explored by a multiscale cartilaginous computational model. In this model, we will test the effect at the tissue level at varying relative abundance of MMP-1 and MMP-9. One of the key computational challenges is developing a physics-based computational model of the diffusion of both enzymes in the tissue. Experimental examination of the enzymatic diffusion in cartilage is lacking. Thus, we employed a spatially randomized diffusion maps to represent the likelihood probability of enzymatic diffusions. A one-to-one map between diffusion and degradation maps were assumed. To achieve this, probabilistic surrogate models of degraded cartilage were created using Latin Hypercube Sampling (LHS). LHS was considered over Monte Carlo Sampling (MCS) herein because LHS techniques generally require fewer samples than traditional MCS for the same accuracy in statistics. The overarching goal is to develop a synthetic *in silico* platform that would allow for the designs of experiments to understand the interplay between the enzymatic ratios and the aggregate mechanics of the degraded cartilage.

## 2 Materials and methods

Studies describing the diffusion characteristics of MMP-1 or MMP-9 into the cartilage are lacking, limiting our ability to construct a physics-based formulation of diffusion equations. Therefore, in this study, enzymatic diffusion was surrogated across the depth-dependent cartilage layers and expressed in probabilistic distribution maps of degraded fibrils via LHS.

The computational construct of the cartilage, in this work, was developed based on the hierarchical morphology observed in collagenous tissue (Adouni and Dhaher 2016; Shirazi and Shirazi-Adl 2008; Tang et al. 2009). A bottom-up formulation hierarchically built the cartilage response at the continuum level, where microfibrils are embedded in a bundle with neo-Hookean matrix to form a fibril, and an aggregate fibrils network is embedded in the neo-Hookean matrix to form the cartilage tissue. Hence, the cartilage is essentially modeled as a fibril-reinforced composite, where the fibril is a microfibril-reinforced composite at a lower length scale. The degradation model was built upon the fact that MMP-1 (col) typically makes the first cleavage in triple-helical collagen, and the initial cleavage unwinds the triple helix, thereby allowing further degradation of the resultant collagen fragments by other MMP-9 (gel). Therefore, we accordingly assume that the properties of non-fibrillar neo-Hookean matrix in the fibrils and tissue, embedding microfibrils and fibrils, respectively, do not or minimally change (degrade) in the current construct, and the degradation exclusively occurred in the microfibrils, not in the non-collagenous matrix.

The computational model (Fig. 1) was constructed by incorporating the results from MD simulations of microfibril degradation into a hyper-elastoplastic fibril-reinforced model of the cartilage (Adouni and Dhaher 2016; Faisal et al. 2019). Three different combinations of MMP-1 and MMP-9 ratios, such as 3:1, 1:1, and 1:3, were considered to examine the role of the relative abundance of MMPs that initiate surface degradation ( $\delta$ ) at collagen fibrils. The MD simulation was conducted by applying tensile force ( $F$ ) on microfibrils and corresponding stress–strain distributions were obtained for intact as well-degraded microfibrils. In addition, an axisymmetric finite element (FE) model under indentation, resembling cartilage samples (plug) used in the reported experimental testing paradigm (Kerin et al. 1998), was simulated. However, the number of indentation-based experiments directing failure mechanisms for cartilage specimens is limited, and the lonely two studies, having different ratios of indenter to plug size (radius), were cited (Kerin et al. 1998; Spahn et al. 2007) and simulated in our prior studies (Faisal et al. 2019). While simulating both experiments in the earlier work showed an increase in the fidelity of our model, the current study opted to provide a synthetic platform for designing required experimental constructs to determine the macro- and micromechanical properties of enzyme-treated cartilages. However, both experimental (Bae et al. 2006; Oyen et al. 2012) and computational (Hayes et al. 1972) modeling show that indentation induces non-uniform strain, where both the magnitude and spatial distribution of strain depend on several variables, including indentation depth and geometry, and size of the cartilage plug (Bae et al. 2007). In the current model, fibril directions exhibited the depth-dependent spatial orientation, beginning

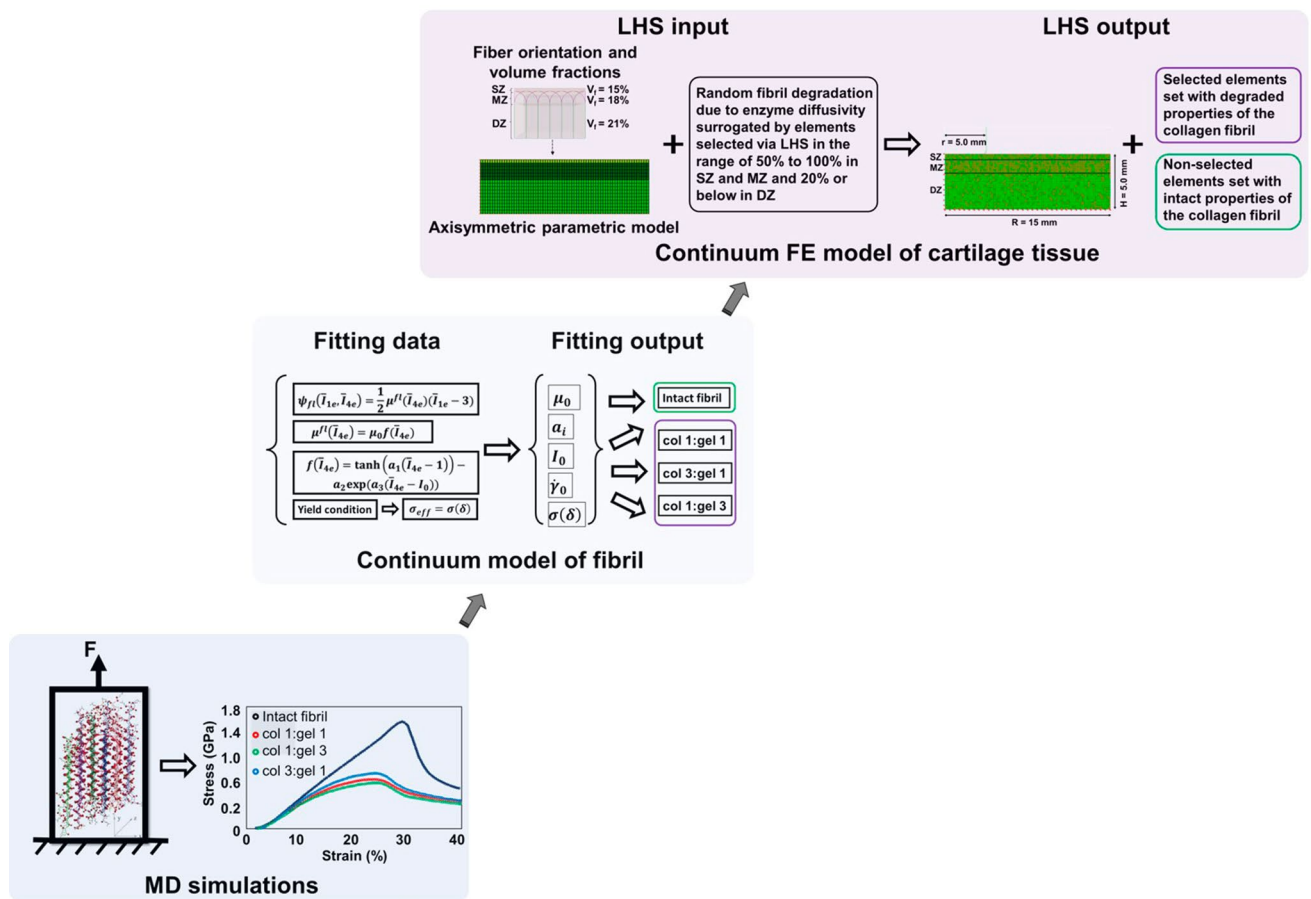


**Fig. 1** Workflow of the adopted multiscale model of articular cartilage degradation mediated by MMPs-1 and 9. MD simulation was conducted via tensile test (tensile force  $F$ ) to capture the effect of MMPs-1 and 9 in microfibril, which is the primary building block of the adopted multiscale model on a continuum scale. The MD simulations provide stress–strain distributions of intact and degraded micro-

fibrils depending on the different MMPs-1 and 9 ratios. The fibril orientations in superficial (SZ), middle (MZ), and deep zones (DZ), along with zone-wise fiber volume fractions, are considered in the axisymmetric model. The degradations due to random diffusivity of the MMPs are surrogated via LHS in the axisymmetric model

at the deep zone, where the collagen fibrils are perpendicular to the subchondral bone and curve gradually to merge parallel (superficial zone) to the surface (Bi et al. 2005; Julkunen et al. 2008) as shown in Fig. 1.

### 2.1 Mechanics of collagen microfibril

The collagen microfibril was modeled as hyper-elastic-plastic material, representing a starting scale in the prior adaptation of hierarchical orders of soft tissue (Adouni and Dhaher 2016; Faisal et al. 2019). The adopted hierarchical construct was formulated based on the multiplicative decomposition of the deformation gradient  $\mathbf{F}$ , which can describe the interplay between the elastic and plastic response (Asaro and Rice 1977; Lee 1969), such that  $\mathbf{F} = \mathbf{F}_e \mathbf{F}_p$ ;  $e$  and  $p$  denote elastic and plastic components,  $\lambda_{fe}$  and  $\lambda_{fp}$  denote elastic and plastic principal fibril stretch,

respectively. In addition, the strain invariants are  $I_1 = \lambda_1^2 + 2\lambda_1^{-1}$  and  $I_4 = \mathbf{C} : \mathbf{n}_o \otimes \mathbf{n}_o = \lambda_f^2 = \lambda_1^2 = \lambda^2$ . In this multiscale construct,  $\lambda_f$  is always assumed to be directed toward the principal strain  $\lambda_1$  in each hierarchy, and therefore,  $\lambda$  is the generalized stretch along the fibril direction in any hierarchical order. Furthermore, the fibrils directions in reference and deformed configurations are  $\mathbf{n}_o$  and  $\mathbf{n}$ , respectively, and are related as  $\mathbf{n} = \frac{F \mathbf{n}_o}{\lambda}$ .  $\mathbf{C} = \mathbf{F}^T \mathbf{F}$  is the right Cauchy-Green deformation tensor. The microfibril level multiplicative decomposition yields a generalized expression of the strain energy function (SEF) as

$$W_{fl}(\bar{I}_{1e}, \bar{I}_{4e}) = \frac{1}{2} \mu^fl(\bar{I}_{4e}) (\bar{I}_{1e} - 3) \tag{1}$$

where  $I_{1e} = \lambda_{1e}^2 + 2\lambda_{1e}^{-1}$  and  $\bar{I}_{4e} = \bar{\mathbf{C}}_e : \mathbf{n}_o \otimes \mathbf{n}_o$ . The shear modulus,  $\mu^fl$ , is a function of elastic microfibril deformation and is expressed by

$$\mu^{fl}(\bar{I}_{4e}) = \mu_o \left( \tanh \left[ a_1 (\bar{I}_{4e} - 1) \right] - a_2 \exp \left[ a_3 (\bar{I}_{4e} - I_o) \right] \right) \tag{2}$$

Derivative of the strain energy with respect to  $\bar{\mathbf{C}}_e$  yields the microfibril stress under uniaxial tension and can be expressed as

$$\sigma_{fl} = -p\mathbf{I} + \left( 2 \frac{\partial W_{fl}}{\partial \bar{I}_{1e}} \bar{\mathbf{B}}_e + 2 \bar{I}_{4e} \frac{\partial W_{fl}}{\partial \bar{I}_{4e}} \mathbf{n} \otimes \mathbf{n} \right) \tag{3}$$

where  $\bar{\mathbf{B}} = \bar{\mathbf{F}}_e \bar{\mathbf{F}}_e^T$  is the left Cauchy-Green tensor, numerically equal to  $\bar{\mathbf{C}}_e$ .

### 2.2 Elasto-plastic modeling of microfibril and softening hyper-elasticity approach

Powell and her colleagues have recently studied the elasto-plastic behavior of microfibril using sequential MC and MD simulations to probe the effect of enzymatic degradation on the structure and mechanics of a single collagen microfibril (Powell et al. 2019). The degradation was imitated by randomly cleaving tropocollagen beads from the healthy microfibril surface, mimicking the MMP-1- and MMP-9-mediated degradation. A collagen microfibril typically exhibits elasto-plastic behavior irrespective of native or degraded states (Buehler 2006, 2008; Malaspina et al. 2017; Powell et al. 2019). Hence, in our earlier study (Faisal et al. 2019), we employed softening hyper-elasticity (Volokh 2007a, 2007b) to represent the elasto-plastic energetics. A constant, *energy limiter*,  $\Phi$ , is defined as the critical failure energy or the maximum strain energy an infinitesimal volume of material can sustain without failure, apprehending the softening (plastic behavior) of microfibril. The energy limiter automatically imposes stress bounds within the constitutive equation and modifies as follows,

$$\sigma_{fl}^{SEF} = -p\mathbf{I} + \left( 2 \frac{\partial W_{fl}}{\partial \bar{I}_{1e}} \bar{\mathbf{B}}_e + 2 \bar{I}_{4e} \frac{\partial W_{fl}}{\partial \bar{I}_{4e}} \mathbf{n} \otimes \mathbf{n} \right) \exp \left( -\frac{W_{fl}^m}{\Phi^m} \right) \tag{4}$$

where  $\Phi$  and  $m$  are positive constants and worked as tuning parameters;  $m$  is a dimensionless parameter that essentially controls the sharpness of the transition from the elastic to the plastic behavior (softening).

The modified expression of microfibril stress in Eq. (4) has been found appropriate to map the MD simulated stress-strain behavior of both native and degraded microfibril to the continuum model. Five microfibril parameters ( $\mu_o, I_o, a_1, a_2, a_3$ ), a subset of unknown materials parameters, are responsible for helping characterize the continuum-based formulation of the fibril mechanics. Softening hyper-elasticity effectively maps the elasto-plastic behavior of collagen

microfibril by adjusting the two tuning parameters (Faisal et al. 2019) in comparison with Bayesian calibration (prior work of our research group), which predicted only the evolution of the elastic properties (Adouni and Dhaher 2016; Salehghaffari and Dhaher 2015). Hence, the microfibril parameters determined by the calibration process [Eq. (4)] are assumed to be more inclusive.

The calibration process introduced in this work was strictly to map the MD simulation results to a continuum model of the fibril at different degradation levels using the formulation [Eq. (4)] of microfibril mechanics presented here. A nonlinear optimization scheme was used to compute the unknown microfibril parameters from the modified microfibril stress, as shown in Eq. (4), for the mechanical response of the three differently degraded microfibrils as computed by the MD simulation. For the nonlinear optimization, the input dataset (MD simulated stress-strain data) was obtained for each of the three relative potencies of the MMPs mixture denoted by col 1:gel 1, col 3: gel 1, and col 1:gel 3. To ensure an unbiased estimate of the microfibril parameters ( $\mu_o, I_o, a_1, a_2, a_3$ ), multiple sets of the five microfibril parameters selected from a plausible range of values (Adouni and Dhaher 2016; Faisal et al. 2019) were considered as the initial inputs to the optimization process. The multiple outputs of the optimization process were then averaged to find the best fit of the microfibril parameters used to characterize the fibril continuum model employed in the subsequent FEA simulations. For the degradation of each MMPs combination, a unique set of microfibril parameters ( $\mu_o, I_o, a_1, a_2, a_3$ ) was estimated. Due to the lack of experimental data on the degraded microfibril mechanics, the calibration of the “continuum-based” model of the microfibril was informed by our prior MD-based simulations (please see Powell et al. 2019).

### 2.3 Multiscale constitutive model

The collagen fibril, which was modeled as the microfibrils reinforced composite, included the descriptions of microfibril and incompressible neo-Hookean matrix. The elastic strain energies of the fibril under extension (*fbt*) and shear (*fs*) were expressed as

$$\begin{cases} W_{fbt}(\bar{I}_4, \bar{I}_{4e}) = v_{fl} W_{fl}(\bar{I}_{1ef}, \bar{I}_{4e}) + v_{ml} \left( \frac{\mu_{fm}}{2} (\bar{I}_{1f} - 3) \right) \\ W_{fs}(\bar{I}_{1f}, \bar{I}_4, \bar{I}_{4e}) = \frac{1}{2} \mu^{effb}(\bar{I}_{4e}) (\bar{I}_{1fb} - \bar{I}_{1f}) \end{cases} \tag{5}$$

The total elastic strain energy density of the fibril was, therefore, expressed as

$$W_{fb}(\bar{I}_{1f}, \bar{I}_4, \bar{I}_{4e}) = W_{fbt}(\bar{I}_4, \bar{I}_{4e}) + W_{fs}(\bar{I}_{1f}, \bar{I}_4, \bar{I}_{4e}) \tag{6}$$

The mathematical framework hierarchically modeled the soft tissue (cartilage) as the fibril reinforced composite material, and the corresponding axial and shear strain energies were written as

$$\begin{cases} W_{tt}(\bar{I}_4, \bar{I}_{4e}) = \nu_f W_{fb}(\bar{I}_{1f}, \bar{I}_4, \bar{I}_{4e}) + \nu_m \left( \frac{\mu_m}{2} (\bar{I}_1 - 3) \right) \\ W_{ts}(\bar{I}_{1f}, \bar{I}_4, \bar{I}_{4e}) = \frac{1}{2} \mu^{eff}(\bar{I}_{4e}) (\bar{I}_1 - \bar{I}_{1f}) \end{cases} \quad (7)$$

The total strain energy of the tissue was defined by

$$W_t(\bar{I}_{1f}, \bar{I}_4, \bar{I}_{4e}) = W_{tt}(\bar{I}_4, \bar{I}_{4e}) + W_{ts}(\bar{I}_{1f}, \bar{I}_4, \bar{I}_{4e}) \quad (8)$$

The total strain energy for the fibril ( $W_{fb}$ ) and tissue ( $W_t$ ) formulations represent the combined axial and shear strains in both constituents. Satisfying the Clausius–Duhem dissipation inequality and the incompressibility constraint, the total stress  $\sigma^t$  was expressed with fibrillar  $\sigma^f$  and nonfibrillar  $\sigma^{nf}$  stress tensors as follows:

$$\begin{cases} \sigma^t = \sigma^{nf} + \sum \sigma_i^f \\ \sigma^{nf} = \frac{2}{J} \left( \bar{I}_1 \frac{\partial W_t}{\partial \bar{I}_1} dev(\bar{\mathbf{B}}) + [E_k \bar{J} (\bar{J} - 1)] I \right) \\ \sigma_i^f = \left\{ \frac{2}{J} \left( \bar{I}_4 \frac{\partial W_t}{\partial \bar{I}_4} dev(\mathbf{n} \otimes \mathbf{n}) + \bar{I}_{4e} \frac{\partial W_t}{\partial \bar{I}_{4e}} dev(\mathbf{n}_e \otimes \mathbf{n}_e) \right) \right\} \text{ if } \bar{I}_{4i} > 1 \\ \sigma_i^f = 0 \text{ if } \bar{I}_{4i} \leq 1 \end{cases} \quad (9)$$

The plastic stress becomes dominant when the effective stress  $\sigma_y^{eff}$  is more than the microfibril yield strength, which in this case varies depending on the degradation by different potency ratios. The effective microfibril stress derived from microfibril strain energy (Tang et al. 2009) activates the progression of plastic stress. The yield stress is connected to the microfibril yield condition as obtained from MD Simulations (i), the plastic strain rate (ii), and the flow resistance (iii) of the tissues as follows:

$$\begin{cases} \sigma_y^{eff} = \frac{4}{3} \bar{I}_{4e} \frac{\partial W_{fb}}{\partial \bar{I}_{4e}} = \sigma_{y(\delta)}^{ff} \quad (i) \\ \dot{\gamma} = \dot{\gamma}_o \left| \frac{\sigma_y^{eff}}{\alpha(t)} \right|^{1/p} sig(\sigma_y^{eff}) \quad (ii) \\ \alpha(t) = \int h \dot{\gamma} f(\alpha) \quad (iii) \end{cases} \quad (10)$$

The elastic part of the deformation gradient is determined by  $\mathbf{F}_e = \mathbf{F} \mathbf{F}_p^{-1}$ , where the plastic deformation gradient is  $f(\lambda_{fp})$ . The stretch,  $\lambda_{fp}$ , has a value of one up to the yield and comes into play beyond the microfibril yield strength. The plastic stretch depends on the plastic strain rate  $\dot{\gamma}$ , which

ultimately controls the plastic part of the deformation gradient. A more detailed description of the evolution of the constitutive model can be found in (Adouni and Dhafer 2016; Tang et al. 2009).

In the current study, Poisson’s ratio of 0.5 was considered for the articular cartilage, and the associated incompressibility of the cartilage was mimicked with an equivalent elastic response by using the equilibrium (drained) modulus of the tissue. The drained modulus was assumed to vary between 0.3 and 1.2 MPa with varying depth when descending from the cartilage surface to the deepest layer at the subchondral bone (Schinagl et al. 1997), and thereby reducing the number of unknown material parameters of the multiscale construct from 13 to 10. Our research group, Adouni et al. (Adouni and Dhafer 2016), conducted a prior study that leveraged experimental data reported in (Akizuki et al. 1986; Eppell et al. 2006; Schinagl et al. 1997). It is important to note that the experimentally calibrated parameters were consistent with the range of data used in several other simulation-based research reports (Guo et al. 2006; Shirazi and Shirazi-Adl

2008; Tang et al. 2010) and were successfully implemented in our prior study that considered different modes of fibrillar degradation (Faisal et al. 2019).

## 2.4 Tissue level synthesis: axisymmetric model with random degradation

A validated finite element model of articular cartilage sample (plug), used in the reported experimental testing paradigm (Fig. 2), was employed here to investigate the role of the relative abundance of MMPs-1 and 9 with an experimentally similar indentation test (Kerin et al. 1998). The indenter was assumed to be a rigid body. The cartilage explant was represented by an axisymmetric model, where the depth-dependent fiber networks at different regions were analogously considered. The axisymmetric parametric model was built upon three-layered, superficial, middle (transitional) and deep layers, tissue morphology with depth-dependent fibril orientation. A cylindrical model with radius  $R = 15$  mm and height of  $H = 5.0$  mm was considered with a rigid indenter size of radius  $r = 5.0$  mm (Kerin et al. 1998). The morphological characteristics, such as the

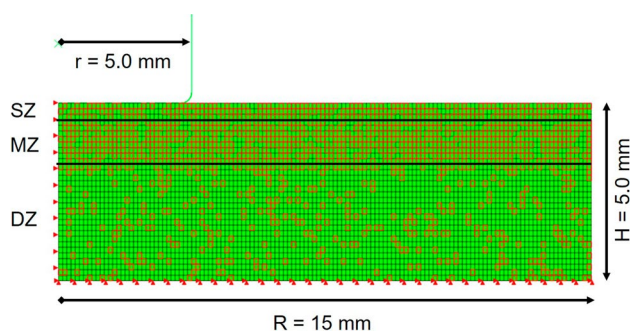


**Fig. 2** An example of a FE model used to simulate the experimental testing paradigm by Kerin et al. (1998) with randomly mapped degraded fibrils. The superficial zone (SZ), middle zone (MZ), and deep zone (DZ) are designed as per (Adouni et al. 2012; Faisal et al. 2019; Shirazi et al. 2008; Wilson et al. 2004) and marked by the black lines. The bottom and left red arrows demonstrate FE boundary conditions and red squares illustrate the random distribution of elements with degraded fibrils in different layers

fibril's length or diameter, were considered indirectly in this investigation. The parameters driving the fibrils' mechanical behavior were optimized to fit the mechanical response of the normal and three differently degraded microfibrils computed by the MD simulation. In the later, the fibril morphology was well defined to minimize its effect on its mechanical response (Powell et al. 2019). The same morphology has been considered over the cartilage since it is embedded in the matrix to generate representative volume elements varied along with the depth via the above-described orientations (Fig. 1). The superficial, transitional, and deep zones were modeled with 15%, 18%, and 21% fibril volume fractions, respectively (Adouni et al. 2012; Faisal et al. 2019; Shirazi et al. 2008; Wilson et al. 2004). The FE model of the cartilage tissue was constructed such that the hyper-elasto-plastic fibrils were embedded in the hyper-elastic (neo-Hookean) matrix. Mesh size of the axisymmetric model was subjected to a sensitivity analysis until a 5% difference in the reaction force was achieved. In the simulated test, the failure stress was primarily validated against the maximum von Mises stress of cartilage tissue with degradation free fibril obtained experimentally by Kerin et al. (1998). Because of the plastic deformation of the fibril beyond the yield stretch, the cartilage tissue's maximum von Mises is considered as the failure stress, which significantly reduces due to fibrillar degradation.

To incorporate the diffusion process of the enzymes into the different layers of the cartilage, we repeated our simulations for each member of a randomly selected set of diffusion maps. In this process, we assumed that the arrival of the enzyme to a spatial location (defined here as a given finite element) is equivalent to the degradation of the fibrils in that specific location. A total of 40 diffusion maps were considered, which likely incorporated the diffusion maps computed

by the traditional diffusion equations. To develop unbiased and near-random diffusion maps (degradation maps), LHS algorithm was used to create varying degradation scenarios across the zones. The primary goal of applying LHS is to create a random distribution to mimic the diffusion of MMPs across the cartilage layers. Here, we choose LHS over MCS because LHS techniques generally require fewer samples than traditional MCS for the same accuracy in statistics. MCS requires many sample sizes to increase the precision of the solution leading to longer computation time. In addition, the sampling technique was considered to facilitate the addition of new training points to the formerly sampled space to improve the precision of the degradation mapped surrogate models. We further assumed that the diffusion of enzymes is more likely to occur in the superficial and middle zones (Lipari and Gerbino 2013; Tetlow et al. 2001), and thus, we set an equal probability of degradation (at least 50%) for the two zones. We also assumed that enzymes would likely not diffuse as effectively in the deep layer (Lipari and Gerbino 2013), and hence, the degradation was limited to 20% (maximum) in the deep zone. The parameter space was mapped using a radial basis function (RBF) to approximate the simulation response (fibril yield strain and cartilage yield stress). The minimum error of the RBF approximation can be achieved with 40 training points (Dhaher et al. 2016; Salehghaffari and Dhaher 2014, 2015).

### 3 Results

The microfibril parameters ( $\mu_o, I_o, a_1, a_2, a_3$ ), required to characterize the microfibril mechanics were determined by nonlinear curve fitting of the MD simulated results using the description of modified microfibril stress [Eq. (4)]. The values of the input parameters are summarized for all three different degradation states in Table 1, and the parameters for the intact fibril can be found in our earlier work (Faisal et al. 2019).

In our prior work, the indentation of the axisymmetric cartilage model with boundary conditions similar to the experiment conducted by Kerin and his colleagues (Kerin et al. 1998) was validated against the maximum von Mises (failure) stress of cartilage tissue with an undegraded fibril. The failure stress of the healthy (control) cartilage tissue was  $\sim 31$  MPa, a value consistent with the earlier study (Faisal et al. 2019). However, the cartilage tissue's maximum von Mises (failure) stress has been significantly reduced in the degraded states. The average values of simulated failure stress are  $16.38 \pm 3.2$  MPa,  $18.06 \pm 4.31$  MPa, and  $19.62 \pm 2.67$  MPa for the three different combinations—(a) col 1:gel 3, (b) col 1:gel 1, and (c) col 3:gel 1, respectively, as shown in Fig. 3. Model predictions indicate that the failure stress is affected by the relative abundance of MMP-1

**Table 1** Fibril material parameters obtained from the data fitting process based on bounding values (Adouni and Dhafer 2016)

Materials parameters		Lower bound	Upper bound	values for col 1:gel 3	values for col 1:gel 1	values for col 3:gel 1
$\mu_o$	Shear modulus of the fibril (MPa)	1000	4000	2136.11	3348.85	3590.20
$I_o$	Secondary stiffening of the fibril	1.6	2.8	2.33	2.59	1.74
$a_1$	Dimensionless fibril parameter 1	0.1	2	1.52	1.97	1.46
$a_2$	Dimensionless fibril parameter 2	100	1000	497.18	769.89	676.27
$a_3$	Dimensionless fibril parameter 3	10	100	55.22	21.35	31.16

and MMP-9 in their mixture and the reductions in failure stress (calculated from the average values of intact tissue failures stress) by 39.8% for the combination denoted by col 1:gel 3, 37.5% for col 1:gel 1, and 36.7% for col 3:gel 1.

The violin plot in Fig. 4 shows the distribution of the yield stress of degraded cartilage for each combination of enzyme (MMPs) mixture as a continuous approximation of the probability density function (PDF), computed using kernel density estimation (KDE). The wider regions of the density plot indicate yield stress values that occur more frequently, and the narrower sections represent a lower probability, indicating yield stress values that occur less frequently. A key advantage that PDFs have over histograms is that the use of a continuous function avoids the issue of having to choose bins. Hence, this gives a more accurate shape of the (yield stress) distribution independent of the number of bins. The violin plot uses KDE to compute an empirical distribution of sample data, and therefore, it better reveals the information contained in the sample and more convincingly suggests multimodality. Distributional differences of the yield stress of the surrogate models of different potency ratios are displayed in the violin plots, displaying each dataset's KDE (smoothed histograms), and are useful for comparing among the three groups. It is apparent that the distribution of yield stress for col 1:gel 3 is bimodal, col 3:gel 1 is skewed, and the distribution is normal for col 1:gel 1.

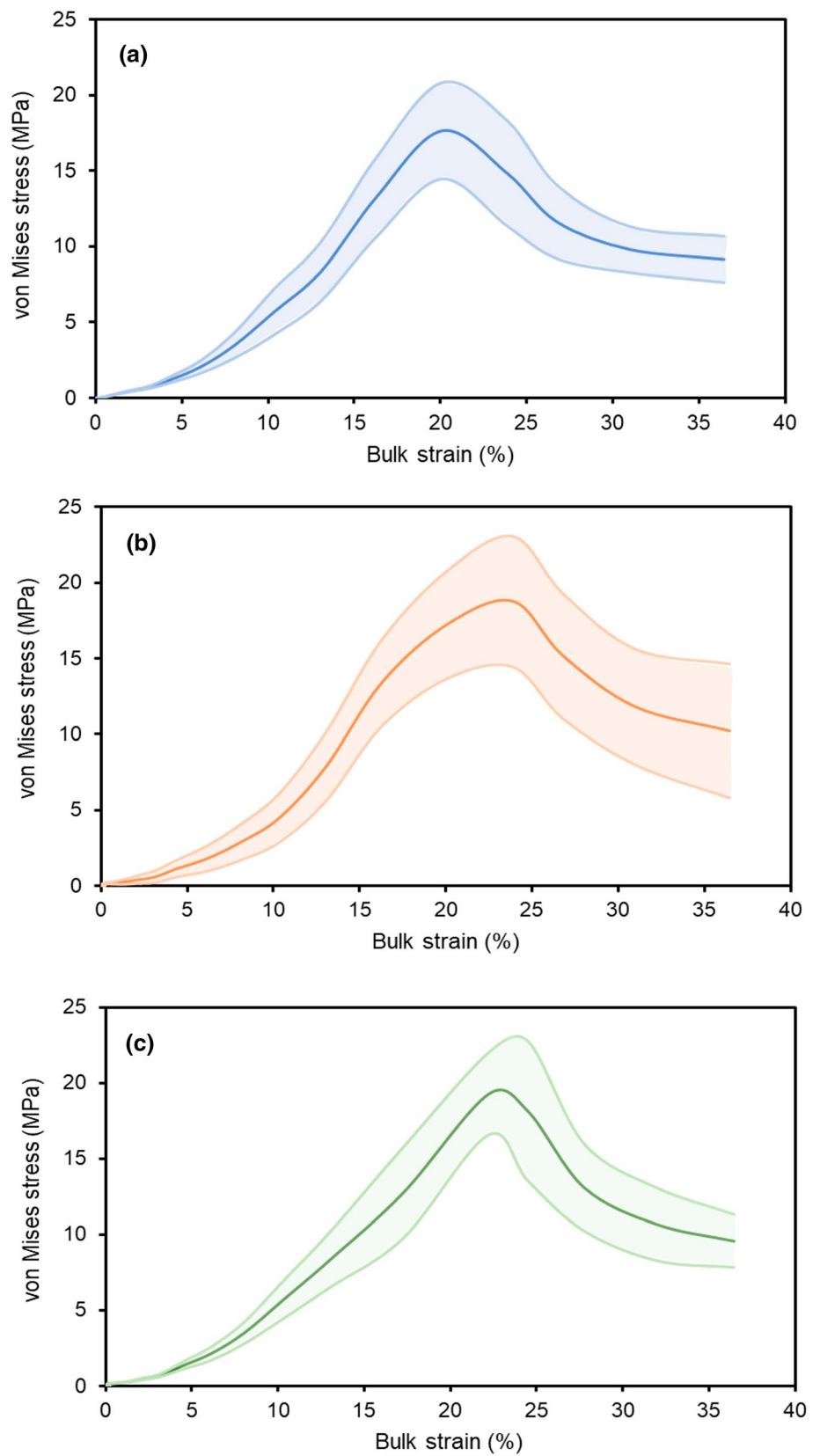
Figure 5 shows examples of plastic principle stretch initiation of fibrils for three different surrogate models (selected at random) of degraded cartilages. The figure illustrates the initiation of plastic changes (local failure) of cartilage as the fibril stretch,  $\lambda_{fp}$ , passed beyond the yield during the simulated indentation test for the three enzyme potency ratios such that col 1:gel 3 (Fig. 5a–c), col 1:gel 1 (Fig. 5d–f), and col 3:gel 1 (Fig. 5g–i). The fibril stretch,  $\lambda_{fp}$ , is unity unless it reaches the yield point and gets a value above one beyond the fibril yield strength, indicating the initiation of plastic deformation. Fibril stretches primarily start in superficial zones and propagate to the middle zone, regardless of the potency of enzyme mixtures. The spatial distribution further indicates that both the amount of degradation and its distribution, as well as the potency of the mixture, influence the fibril yield, which we consider as the local failure. For more equally distributed degraded fibrils across the zones

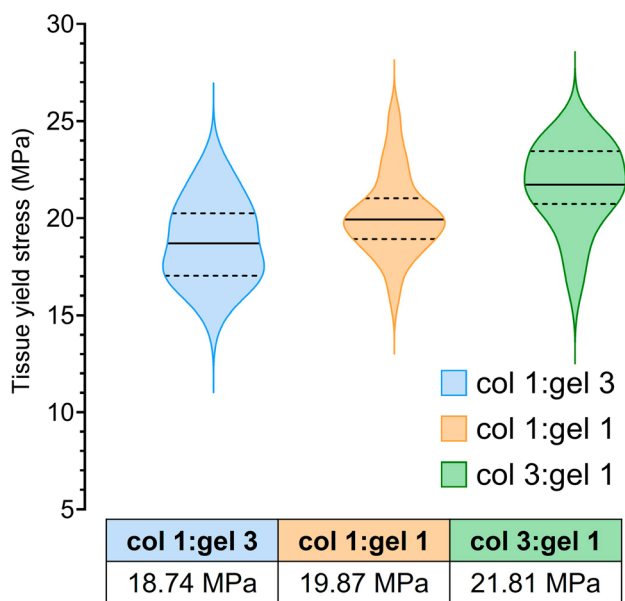
(Fig. 5a, d, and g), the yield initiates in the fibril at the applied bulk strain of ~24% and above. On the contrary, the yield starts much earlier between ~13% and ~17% of applied bulk strain to cartilage tissue, when the degraded fibrils are concentrated primarily in the superficial and middle layers (Fig. 5c, f, and i). It is, therefore, evident that the diffusivity of enzymes, causing random degradation in fibril, plays a crucial role along with the enzyme potency in influencing the fibril yield. The nonparametric Kruskal–Wallis test ( $\alpha = 0.05$ ) was used to compare the yield initiation of fibril (local failure) among the cartilage degraded with different potency of enzymes. Kruskal–Wallis analysis indicated that the yield initiation was significantly different among the groups ( $p < 0.05$ ).

Figure 6 shows the spatial distribution (propagation) of plastic changes (failure) of degraded cartilage in terms of fibril stretch,  $\lambda_{fp}$ , at 36% of applied bulk strain during the simulated indentation test. While Fig. 5 shows the initiation of fibril plastic stretch, Fig. 6 shows its progression at the maximum applied bulk strain (36% strain) considered herein. This allows us to compare the end effect of all the parameters that cumulatively influence cartilage tissue behavior in a degraded state. The degradation was initiated from the central zone on the surface and then propagated to the middle zone (Fig. 6). As a result, the degradation is spanned ~42%, ~60%, and ~80% away from the axis of symmetry of the indenter for the different degradation mapping of the cartilage tissue degenerated with enzyme potency of col 1:gel 3 (Figs. 6a–c). The approximate spanning of degradation is ~40%, ~47%, and ~60% away from the indenter's axis of symmetry for the considered degradation mapping due to enzyme potency of col 1:gel 1 (Figs. 6d–f). The spatial degradation is spanned less for the cartilage degraded with the enzyme of the potency of col 3:gel 1, where the degradation is extended away up to ~20%, ~35%, and ~45% from the center of indenter for different degradation mapping. Therefore, it is evident that both degradation mapping and potency of enzyme mixtures influence the spatial propagation of the failure behavior of fibril as well as the cartilage.

Figure 7 shows the distributions of fibril yield (local failure) in applied bulk strain for each concentration of enzyme mixtures. As indicated, the initiations of local failures are mostly concentrated on the superficial zone for col 1:gel

**Fig. 3** Stress variation in articular cartilage as per the simulated indentation test for randomly mapped fibril degraded by an enzyme with a potency of **a** col 1:gel 3, **b** col 1:gel 1, and **c** col 3:gel 1. The graph shows average von Mises stress with upper and lower bounds ( $\pm$ SD) subjected to 36% of bulk strain for the models generated with LHS,  $N=40$





**Fig. 4** Violin plot showing tissue yield stress distributions for the three different potency ratios in MMP-1 (col) and MMP-9 (gel) mixtures used in this study. The solid line represents median; dotted lines are for 1st (bottom) and 3rd (top) quartiles. Median tissue yield stress for each potency ratio is reported in tabular format

3 and are spread over superficial and middle zones for the other two combinations of enzymatic ratios. A Kruskal–Wallis test revealed that there was a significant effect of enzymatic concentration on the bulk strain associated with the initiation of local failure ( $H(2) = 16.49, p < 0.01$ ) with col 1:gel 3 mixture express failure at lower bulk strain with the highest level of local failures express at elements closer to the edge of the superficial layer (the statistical distribution in the inset at the right top corner of Fig. 7). The distribution of failure initiation is more symmetric for the equal concentration ratio (col 1:gel 1) and asymmetric for the other two with unequal potency ratios. The data are statistically more dispersed and scattered in col 3:gel 1 and col 1:gel 3. The density distributions of the locations of elements with yielded fibrils are shown for each potency ratio.

#### 4 Discussion

The objective of this study was to develop a computational model of the mixed effect of fibril degradation mediated by two key enzymes (collagenase and gelatinase) on cartilage mechanics with probabilistic expressions of enzymatic diffusions. Our simulation results revealed that probabilistic

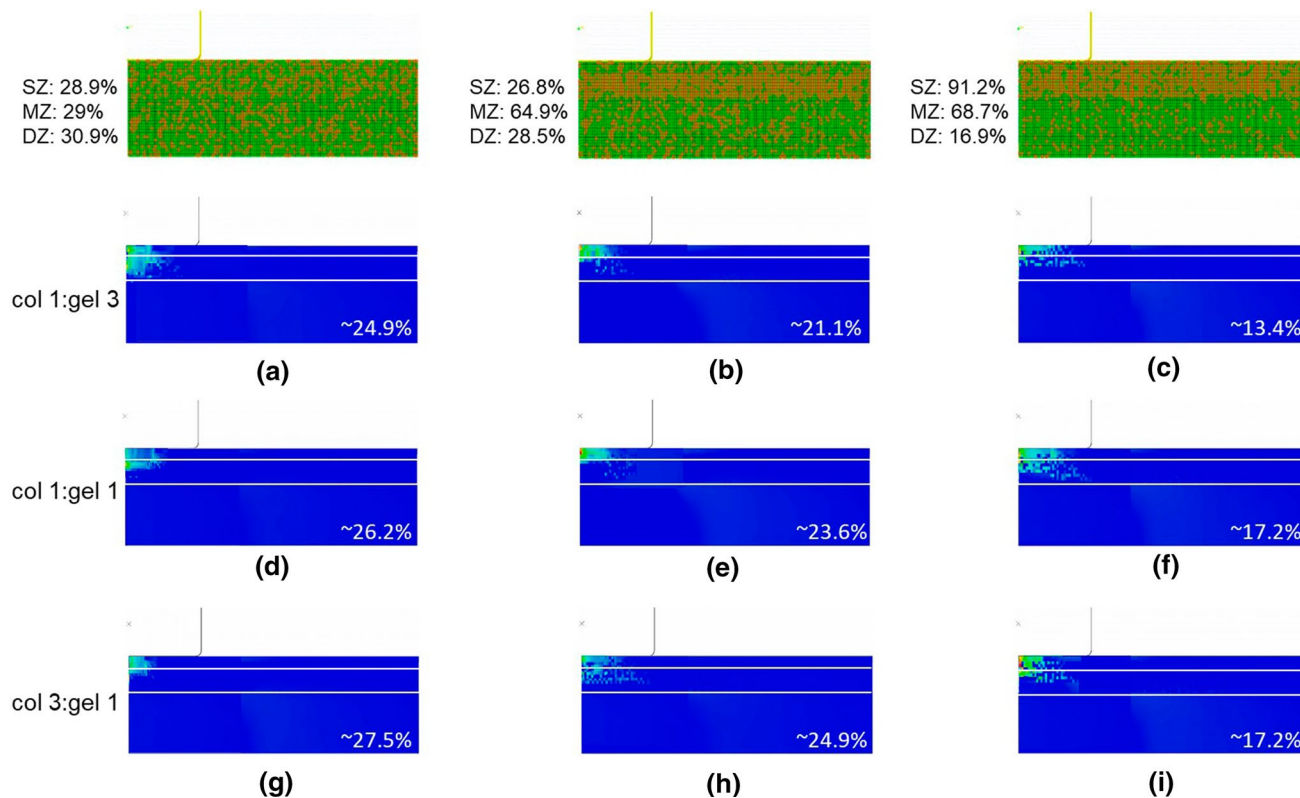


**Fig. 5** Initiation of cartilage plastic changes represented by the distribution of plastic fibril principal stretch for the enzymatic degradation with the potency of col 1:gel 3 **a–c**, col 1:gel 1 **d–f** and col 3:gel 1 **g–i**

for three selected at random diffusion maps. The solid white lines show the superficial zone (SZ), middle zone (MZ), and deep zone (DZ) from the top

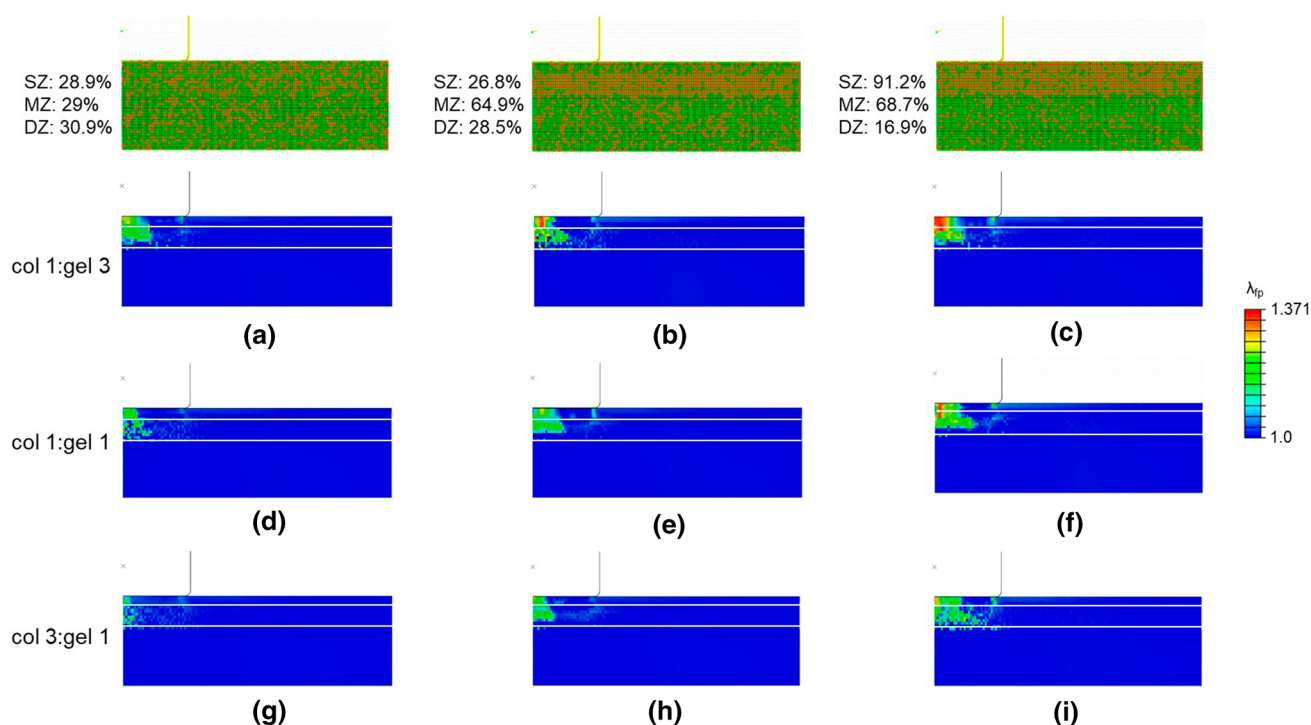


**Fig. 6** Propagation of cartilage plastic changes represented by the distribution of the maximum plastic fibril principal stretch ( $\lambda_{fp}$ ) for the enzymatic degradation for the three relative potencies of enzymes (col 1:gel 3 **a–c**, col 1:gel 1 **d–f** and col 3:gel 1 **g–i**) at 36% of applied

bulk strain for three at randomly selected diffusion maps. The solid white lines show the superficial (SZ), middle (MZ), and deep (DZ) zones from the top

mapping of degraded fibrils plays a major role in defining the mechanical integrity of the articular cartilage. Specifically, our analysis indicated that the variation in degraded fibrillar distributions in superficial and middle layers plays a detrimental role in yield behavior at the tissue level. Our results also indicated that examination of the relative abundance of the two enzymes at the fibril level is manifested at the tissue level, a higher relative abundance of gelatinase to collagenase results in structurally softer cartilage. While informative, our findings highlight the significance of the diffusion characteristics of these two enzymes on the link between fibril and tissue levels failures. Thus, the *in silico*-based observations highlight the need for *in vitro* experiments to characterize the individual and combined enzymatic diffusion characteristics in cartilage.

The earliest sign of visible degeneration in the articular surface is localized fibrillation of the superficial layer of the articular cartilage. Prior experiments showed that fibrillation, clefts, and disintegration of collagen fibril network occurred in the superficial layer in the early stage of cartilage degeneration (Clarke 1971; Hong and Henderson 1996; Hwang et al. 1992; Panula et al. 1998; Saxena et al. 1991). Thus, it has been proposed that yield typically initiates at the superficial layer (zone) and then propagates to the middle and deep layers (Clarke 1971; Saxena et al. 1991). Our

model simulations also indicated that the fibril yield (local failure) begins at the superficial layers (Figs. 5c, f, and i), a spatial bias independent of the relative abundance of the enzymes. However, the initiation of yield (local failure) in the middle layer showed varied spatial patterns for the different relative abundances of the two enzymes. It is likely that the random collagen network in the middle layer creates complex diffusion characteristics and makes the local failure difficult to predict (Hong et al. 2015).

In the current computational model, we assumed that the degradation is isolated to the collagen fibril network and not in the non-fibrillar matrix. However, evidence in the literature indicates that the access of the MMPs to collagen is made possible by the degradation of the aggrecans/procollagens via aggrecanases, A Disintegrin and Metalloprotease with Thrombospondin Motifs (ADAMTS) (Gendron et al. 2007; Nagase and Kashiwagi 2003; Roughley and Mort 2014). While, functionally, extracellular matrix degradation constructs in terms of a strain energy function formulations have been proposed (Eskelinen et al. 2019; Hosseini et al. 2014; Liu et al. 2020; Mononen et al. 2016), molecular dynamic-based analyses of the action of ADAMTS on aggrecans and its effect on the basic mechanics of the extracellular matrix (non-collagenous) are lacking. The diffusion of pro-inflammatory cytokines from the synovial fluid into cartilage

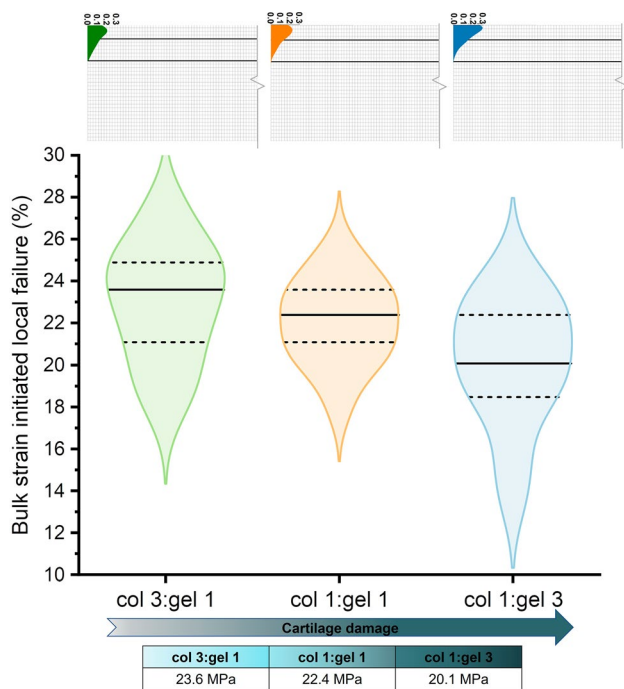


**Fig. 7** Violin plots showing bulk strain initiated fibril local failure (fibril plastic stretch),  $\lambda_{fp} > 1$ , among different concentration ratios of MMP-1 (col) and MMP-9 (gel). Violin plots display median values (central horizontal line), first (bottom) and third quartiles (top). Density distributions of elements where fibril yield (local failure) initiated in the surrogate models of each enzyme group are shown (half of the axisymmetric model) on top of each violin plot. The solid black lines show the superficial, middle, and deep zones from the top. In addition, the median yield stress for each potency ratio is reported (bottom)

(Kar et al. 2016a, c; Krishnan and Grodzinsky 2018; Loeser et al. 2012) leads to proteolysis of cartilage matrix during joint inflammation in OA. Kar and coworkers (Kar et al. 2016a, c) developed a computational model addressing the diffusion of pro-inflammatory cytokines, IL-1, into cartilage and the subsequent degeneration of cartilage tissue. The inflammatory cytokines upregulate ADAMTS and MMPs, which degrade both aggrecans (the main PG in articular cartilage) and collagens.

In our recent experimental work (Mixon et al. 2022), we observed that col 3:gel 1 is more detrimental than col 1:gel 3, which in contrast exhibits a more degrading effect in our current study. Pathologically, MMPs have a variety of targets and can degrade collagen and ECM components. MMP-9 is the most complex member of the MMP family with its proteolytic activity. Practically, the gelatinases have a broad substrate specificity and contribute, together with collagenases, to the degradation and digestion of fibrillar collagens as well as proteoglycans (PG). Hence, the stabilizing role of PG was compromised, which has been preserved in our computational model since we have not considered any degradation

and digestion of PG but collagen only. Furthermore, in healthy tissues, aggregating proteoglycans occupying the interfibrillar zone intuitively act as a barrier to protect the cross-linked collagen fibrils from enzymatic denaturation (Smith 1999). With the aggregating PG barrier compromised by the presence of MMP-9, collagenase (MMP-1) receives access to the type II collagen fibrils, and thereby initiating more degradation of collagen experimentally. Hosseini et al. (Hosseini et al. 2014) also suggest that both the intact fibrillar network and matrix may be mutually protective against damage and that damage can promote cartilage failure. In contrast, the current computational model has been built upon prior works (Malaspina et al. 2017; Powell et al. 2019; Rosenblum et al. 2010; Sarkar et al. 2012) and we accordingly assume that the non-collagenous neo-Hookean matrix properties in fibrils or tissue were not affected by the enzymes considered in this study. In the context of the bottom-up approach considered herein, MD-based characterization of failure of the PG aggregates (matrix) via PG-specific enzymes is computationally intractable. Therefore, combined with the complexity of the molecular diffusion in the tissue, the inclusion of aggrecanases' action is beyond the scope of this examination.

The current construct has been further formulated hierarchically with a bottom-up approach, ignoring poro-elastic explicit effect due to the fluid content of cartilage, a simplifying assumption to reduce computational cost (Kazemi et al. 2013). However, to reflect the incompressibility of the articular cartilage during the transient (short-term) biphasic response, an equivalent elastic response was determined by using the equilibrium (drained) modulus of the tissue and Poisson's ratio of 0.5 (Adouni and Dhaher 2016; Faisal et al. 2019). In this work, we assumed a minimum of 50% of fibrils at the superficial layer were degraded as commensurate with prior studies (Kar et al. 2016a), and we further extended this limiting assumption to middle layers because of the absence of any experimental diffusion map. Finally, variation in failure stress in cartilage depends on many factors such as maturation, aging, location, collagen types, and composition (Danso et al. 2014; Eleswarapu et al. 2011; Williamson et al. 2003), which were not included in the current construct.

Exploring the effect of degraded fibrils on cartilage mechanics is experimentally challenging. Studies showed that higher fibril degeneration and localization of the tissue experience excessive stress (Mononen et al. 2016). Furthermore, several reports indicate that aggrecan (matrix) protects collagen fibrils in cartilage, and aggrecanase is a required precursor to the degraded aggrecan for the exposure of the fibrils to the collagenase (Kar et al. 2016b; Li et al. 2015; Pratta et al. 2003). In addition, the deep layer may remain unaffected when the cartilage is treated with enzymes, as evident in diffusion simulation and experiment (Arbabi et al.

2015; Mixon et al. 2021, 2022), and the fibril network may be mechanically compromised in the middle and deep layers before any visible degradation becomes apparent at the surface (Hosseini et al. 2014). Fibril degradation mediated by enzymatic processes depends on many factors, among which the diffusion of the enzymes into the cartilaginous tissue bears the spatial characteristics (Arbabi et al. 2015; Kar et al. 2016a; Li et al. 2015). This study attempted to address this issue using a probabilistic diffusion map. The current in silico analysis will provide insights into the design of experimental paradigms to identify the parameters necessary to increase the fidelity of the multi-scale modeling of cartilage degradation constructs.

**Acknowledgements** This work, in part, is supported by a grant (#U01 EB015410-01A1) from the National Institute of Health (NIH).

**Author contributions** All authors have read and approved this submission; TF carried out analyses, all (TF, MA, and YD) participated in the definition, design, and development of the work, and finally, the manuscript was written and reviewed by all authors (TF, MA, and YD).

## Declarations

**Conflict of interest** The authors declare no conflict of interest.

## References

- Adouni M, Dhaher YY (2016) A multi-scale elasto-plastic model of articular cartilage. *J Biomech* 49:2891–2898
- Adouni M, Shirazi-Adl A, Shirazi R (2012) Computational biodynamics of human knee joint in gait: From muscle forces to cartilage stresses. *J Biomech* 45:2149–2156. <https://doi.org/10.1016/j.jbiomech.2012.05.040>
- Akizuki S, Mow VC, Müller F, Pita JC, Howell DS, Manicourt DH (1986) Tensile properties of human knee joint cartilage: I. Influence of ionic conditions, weight bearing, and fibrillation on the tensile modulus. *J Orthop Res* 4:379–392. <https://doi.org/10.1002/jor.1100040401>
- Arbabi V, Pouran B, Weinans H, Zadpoor A (2015) Transport of neutral solute across articular cartilage: the role of zonal diffusivities. *J Biomech Eng* 137:071001
- Asaro RJ, Rice JR (1977) Strain localization in ductile single crystals. *J Mech Phys Solids* 25:309–338. [https://doi.org/10.1016/0022-5096\(77\)90001-1](https://doi.org/10.1016/0022-5096(77)90001-1)
- Bae WC, Lewis CW, Levenston ME, Sah RL (2006) Indentation testing of human articular cartilage: effects of probe tip geometry and indentation depth on intra-tissue strain. *J Biomech* 39:1039–1047. <https://doi.org/10.1016/j.jbiomech.2005.02.018>
- Bae WC, Schumacher BL, Sah RL (2007) Indentation probing of human articular cartilage: effect on chondrocyte viability. *Osteoarthr Cartil* 15:9–18. <https://doi.org/10.1016/j.joca.2006.06.007>
- Barbour KE, Helmick CG, Theis KA, Murphy LB, Hootman JM, Brady TJ, Cheng YJ (2013) Prevalence of doctor-diagnosed arthritis and arthritis-attributable activity limitation—United States, 2010–2012 MMWR Morbidity and mortality weekly report 62:869
- Bi X, Li G, Doty S, Camacho N (2005) A novel method for determination of collagen orientation in cartilage by Fourier transform infrared imaging spectroscopy (FT-IRIS). *Osteoarthr Cartil* 13:1050–1058
- Buckwalter JA, Mankin HJ (1998) Articular cartilage: degeneration and osteoarthritis, repair, regeneration, and transplantation. *Inst Course Lect* 47:487–504
- Buehler MJ (2006) Nature designs tough collagen: Explaining the nanostructure of collagen fibrils. *Proc Natl Acad Sci* 103:12285–12290. <https://doi.org/10.1073/pnas.0603216103>
- Buehler MJ (2008) Nanomechanics of collagen fibrils under varying cross-link densities: Atomistic and continuum studies. *J Mech Behav Biomed Mater* 1:59–67. <https://doi.org/10.1016/j.jmbbm.2007.04.001>
- Clarke IC (1971) articular cartilage: a review and scanning electron microscope study. *Bone Joint J* 53:732–750
- Danso EK, Honkanen JTJ, Saarakkala S, Korhonen RK (2014) Comparison of nonlinear mechanical properties of bovine articular cartilage and meniscus. *J Biomech* 47:200–206. <https://doi.org/10.1016/j.jbiomech.2013.09.015>
- Dhaher YY, Salehghaffari S, Adouni M (2016) Anterior laxity, graft-tunnel interaction and surgical design variations during anterior cruciate ligament reconstruction: a probabilistic simulation of the surgery. *J Biomech* 49:3009–3016
- Eleswarapu SV, Responde DJ, Athanasiou KA (2011) Tensile properties, collagen content, and crosslinks in connective tissues of the immature knee joint. *PLoS ONE* 6:e26178
- Eppell SJ, Smith BN, Kahn H, Ballarini R (2006) Nano measurements with micro-devices: mechanical properties of hydrated collagen fibrils. *J R Soc Interface* 3:117–121. <https://doi.org/10.1098/rsif.2005.0100>
- Eskelinen ASA, Mononen ME, Venäläinen MS, Korhonen RK, Tanska P (2019) Maximum shear strain-based algorithm can predict proteoglycan loss in damaged articular cartilage. *Biomech Model Mechanobiol* 18:753–778. <https://doi.org/10.1007/s10237-018-01113-1>
- Faisal TR, Adouni M, Dhaher YY (2019) The effect of fibrillar degradation on the mechanics of articular cartilage: a computational model. *Biomech Model Mechanobiol* 18:733–751
- Gendron C et al (2007) Proteolytic activities of human ADAMTS-5: comparative studies with ADAMTS-4. *J Biol Chem* 282:18294–18306
- Grenier S, Bhargava MM, Torzilli PA (2014) An in vitro model for the pathological degradation of articular cartilage in osteoarthritis. *J Biomech* 47:645–652
- Guo ZY, Peng XQ, Moran B (2006) A composites-based hyperelastic constitutive model for soft tissue with application to the human annulus fibrosus. *J Mech Phys Solids* 54:1952–1971. <https://doi.org/10.1016/j.jmps.2006.02.006>
- Hayes WC, Keer LM, Herrmann G, Mockros LF (1972) A mathematical analysis for indentation tests of articular cartilage. *J Biomech* 5:541–551. [https://doi.org/10.1016/0021-9290\(72\)90010-3](https://doi.org/10.1016/0021-9290(72)90010-3)
- Hong S, Henderson C (1996) Articular cartilage surface changes following immobilization of the rat knee joint. *Cells Tissues Organs* 157:27–40
- Hong J, Evans TM, Mente PL (2015) Study on the damage mechanism of articular cartilage based on the fluid–solid coupled particle model. *Adv Mech Eng* 7:1687814015581264
- Hosseini SM, Wilson W, Ito K, van Donkelaar CC (2014) A numerical model to study mechanically induced initiation and progression of damage in articular cartilage. *Osteoarthr Cartil* 22:95–103. <https://doi.org/10.1016/j.joca.2013.10.010>
- Hwang W, Li B, Jin L, Ngo K, Schachar N, Hughes G (1992) Collagen fibril structure of normal, aging, and osteoarthritic cartilage. *J Pathol* 167:425–433
- Julkunen P, Wilson W, Jurvelin JS, Rieppo J, Qu C-J, Lammi MJ, Korhonen RK (2008) Stress–relaxation of human patellar articular cartilage in unconfined compression: prediction of

- mechanical response by tissue composition and structure. *J Biomech* 41:1978–1986
- Kar S, Smith DW, Gardiner BS, Grodzinsky AJ (2016a) Systems based study of the therapeutic potential of small charged molecules for the inhibition of IL-1 mediated cartilage degradation. *PLoS ONE* 11:e0168047. <https://doi.org/10.1371/journal.pone.0168047>
- Kar S, Smith DW, Gardiner BS, Li Y, Wang Y, Grodzinsky AJ (2016b) Modeling IL-1 induced degradation of articular cartilage. *Arch Biochem Biophys* 594:37–53. <https://doi.org/10.1016/j.abb.2016.02.008>
- Kazemi M, Dabiri Y, Li L (2013) Recent advances in computational mechanics of the human knee joint. *Computational and Mathematical Methods in Medicine* 2013
- Kerin AJ, Wisnom MR, Adams MA (1998) The compressive strength of articular cartilage. *Proc Inst Mech Eng Part H J Eng Med* 212:273–280. <https://doi.org/10.1243/0954411981534051>
- Krishnan Y, Grodzinsky AJ (2018) Cartilage diseases. *Matrix Biol* 71:51–69
- Lee EH (1969) Elastic-plastic deformation at finite strains. *J Appl Mech* 36:1–6. <https://doi.org/10.1115/1.3564580>
- Li Y, Wang Y, Chubinskaya S, Schoeberl B, Florine E, Kopesky P, Grodzinsky AJ (2015) Effects of insulin-like growth factor-1 and dexamethasone on cytokine-challenged cartilage: relevance to post traumatic osteoarthritis osteoarthritis and cartilage / OARS. *Osteoarthr Res Soc* 23:266–274. <https://doi.org/10.1016/j.joca.2014.11.006>
- Lipari L, Gerbino A (2013) Expression of gelatinases (MMP-2, MMP-9) in human articular cartilage. *Int J Immunopathol Pharmacol* 26:817–823
- Liu D, Ma S, Stoffel M, Markert B (2020) A biphasic visco-hyperelastic damage model for articular cartilage: application to micromechanical modelling of the osteoarthritis-induced degradation behaviour. *Biomech Model Mechanobiol* 19:1055–1077
- Loeser RF, Goldring SR, Scanzello CR, Goldring MB (2012) Osteoarthritis: a disease of the joint as an organ. *Arthr Rheum* 64:1697
- Malaspina DC, Szleifer I, Dhaher Y (2017) Mechanical properties of a collagen fibril under simulated degradation. *J Mech Behav Biomed Mater* 75:549–557. <https://doi.org/10.1016/j.jmbbm.2017.08.020>
- Mixon A, Savage A, Bahar-Moni AS, Adouni M, Faisal T (2021) An in vitro investigation to understand the synergistic role of MMPs-1 and 9 on articular cartilage biomechanical properties. *Sci Rep* 11:14409. <https://doi.org/10.1038/s41598-021-93744-1>
- Mixon A, Bahar-Moni AS, Faisal TR (2022) Mechanical characterization of articular cartilage degraded combinedly with MMP-1 and MMP-9. *J Mech Behav Biomed Mater*. <https://doi.org/10.1016/j.jmbbm.2022.105131>
- Mononen ME, Tanska P, Isaksson H, Korhonen RK (2016) A novel method to simulate the progression of collagen degeneration of cartilage in the knee: data from the osteoarthritis initiative. *Sci Rep* 6:21415
- Nagase H, Kashiwagi M (2003) Aggrecanases and cartilage matrix degradation. *Arthr Res Ther* 5:94–103. <https://doi.org/10.1186/ar630>
- Oyen ML, Shean TA, Strange DG, Galli M (2012) Size effects in indentation of hydrated biological tissues. *J Mater Res* 27:245–255
- Panula HE, Hyttinen MM, Arokoski JP, Långsjö TK, Pelttari A, Kiviranta I, Helminen HJ (1998) Articular cartilage superficial zone collagen birefringence reduced and cartilage thickness increased before surface fibrillation in experimental osteoarthritis. *Ann Rheum Dis* 57:237–245
- Powell B, Malaspina DC, Szleifer I, Dhaher Y (2019) Effect of collagenase–gelatinase ratio on the mechanical properties of a collagen fibril: a combined Monte Carlo–molecular dynamics study. *Biomech Model Mechanobiol* 18:1809–1819. <https://doi.org/10.1007/s10237-019-01178-6>
- Pratta MA et al (2003) Aggrecan protects cartilage collagen from proteolytic cleavage. *J Biol Chem* 278:45539–45545. <https://doi.org/10.1074/jbc.M303737200>
- Punzi L, Galozzi P, Luisetto R, Favero M, Ramonda R, Oliviero F, Scanu A (2016) Post-traumatic arthritis: overview on pathogenic mechanisms and role of inflammation RMD. *Open* 2:e000279–e000279. <https://doi.org/10.1136/rmdopen-2016-000279>
- Rosenblum G, Van den Steen PE, Cohen SR, Bitler A, Brand DD, Opendakker G, Sagi I (2010) Direct visualization of protease action on collagen triple helical structure. *PLoS ONE* 5:e11043
- Roughley PJ, Mort JS (2014) The role of aggrecan in normal and osteoarthritic cartilage. *J Exp Orthop* 1:8. <https://doi.org/10.1186/s40634-014-0008-7>
- Saarakkala S, Töyräs J, Hirvonen J, Laasanen MS, Lappalainen R, Jurvelin JS (2004) Ultrasonic quantitation of superficial degradation of articular cartilage. *Ultrasound Med Biol* 30:783–792
- Salehghaffari S, Dhaher YY (2014) A model of anterior cruciate ligament reconstructive surgery: a validation construct and computational insights. *J Biomech* 47:1609–1617. <https://doi.org/10.1016/j.jbiomech.2014.03.003>
- Salehghaffari S, Dhaher YY (2015) A phenomenological contact model: Understanding the graft-tunnel interaction in anterior cruciate ligament reconstructive surgery. *J Biomech* 48:1844–1851. <https://doi.org/10.1016/j.jbiomech.2015.04.034>
- Sarkar SK, Marmer B, Goldberg G, Neuman KC (2012) Single-molecule tracking of collagenase on native type I collagen fibrils reveals degradation mechanism. *Curr Biol* 22:1047–1056
- Saxena RK, Sahay KB, Guha SK (1991) Morphological changes in the bovine articular cartilage subjected to moderate and high loadings. *Cells Tissues Organs* 142:152–157
- Schinagl RM, Gurskis D, Chen AC, Sah RL (1997) Depth-dependent confined compression modulus of full-thickness bovine articular cartilage. *J Orthop Res* 15:499–506. <https://doi.org/10.1002/jor.1100150404>
- Schmidt MB, Mow VC, Chun LE, Eyre DR (1990) Effects of proteoglycan extraction on the tensile behavior of articular cartilage. *J Orthop Res* 8:353–363
- Shirazi R, Shirazi-Adl A (2008) Deep vertical collagen fibrils play a significant role in mechanics of articular cartilage. *J Orthop Res* 26:608–615. <https://doi.org/10.1002/jor.20537>
- Shirazi R, Shirazi-Adl A, Hurtig M (2008) Role of cartilage collagen fibrils networks in knee joint biomechanics under compression. *J Biomech* 41:3340–3348
- Smith RL (1999) Degradative enzymes in osteoarthritis. *Front Biosci* 4:D704–712. <https://doi.org/10.2741/a388>
- Spahn G, Kahl E, Klinger Hans M, Mückley T, Günther M, Hofmann Gunther O (2007) Mechanical behavior of intact and low-grade degenerated cartilage/Mechanische Eigenschaften von intaktem und niedriggradig geschädigtem Knorpel <https://doi.org/10.1515/BMT.2007.039>
- Tang H, Buehler MJ, Moran B (2009) A constitutive model of soft tissue: from nanoscale collagen to tissue continuum. *Ann Biomed Eng* 37:1117–1130. <https://doi.org/10.1007/s10439-009-9679-0>
- Tang Y, Ballarini R, Buehler MJ, Eppell SJ (2010) Deformation micro-mechanisms of collagen fibrils under uniaxial tension. *J R Soc Interface* 7:839–850. <https://doi.org/10.1098/rsif.2009.0390>
- Tetlow LC, Adlam DJ, Woolley DE (2001) Matrix metalloproteinase and proinflammatory cytokine production by chondrocytes of human osteoarthritic cartilage: associations with degenerative changes. *Arthritis Rheum* 44:585–594
- Töyräs J, Rieppo J, Nieminen M, Helminen H, Jurvelin J (1999) Characterization of enzymatically induced degradation of articular cartilage using high frequency ultrasound. *Phys Med Biol* 44:2723

- Volokh KY (2007a) Hyperelasticity with softening for modeling materials failure. *J Mech Phys Solids* 55:2237–2264. <https://doi.org/10.1016/j.jmps.2007.02.012>
- Volokh KY (2007b) Softening hyperelasticity for modeling material failure: Analysis of cavitation in hydrostatic tension. *Int J Solids Struct* 44:5043–5055. <https://doi.org/10.1016/j.ijsolstr.2006.12.022>
- Wang Q et al (2008) Real-time ultrasonic assessment of progressive proteoglycan depletion in articular cartilage. *Ultrasound Med Biol* 34:1085–1092
- Weiss C, Mirow S (1972) An ultrastructural study of osteoarthritic changes in the articular cartilage of human knees. *JBJS* 54:954–972
- Williamson AK, Chen AC, Masuda K, Thonar EJMA, Sah RL (2003) Tensile mechanical properties of bovine articular cartilage: variations with growth and relationships to collagen network components. *J Orthop Res* 21:872–880. [https://doi.org/10.1016/S0736-0266\(03\)00030-5](https://doi.org/10.1016/S0736-0266(03)00030-5)
- Wilson W, van Donkelaar CC, van Rietbergen B, Ito K, Huiskes R (2004) Stresses in the local collagen network of articular cartilage: a poroviscoelastic fibril-reinforced finite element study. *J Biomech* 37:357–366. [https://doi.org/10.1016/S0021-9290\(03\)00267-7](https://doi.org/10.1016/S0021-9290(03)00267-7)

**Publisher's Note** Springer Nature remains neutral with regard to jurisdictional claims in published maps and institutional affiliations.

Springer Nature or its licensor holds exclusive rights to this article under a publishing agreement with the author(s) or other rightsholder(s); author self-archiving of the accepted manuscript version of this article is solely governed by the terms of such publishing agreement and applicable law.